Direct Dynamics Trajectory Study of the Reaction of Formaldehyde Cation with D₂: Vibrational and Zero-Point Energy Effects on Quasiclassical Trajectories[†]

Jianbo Liu

Department of Chemistry, University of Utah, 315 S 1400 E, Salt Lake City, Utah 84112

Kihyung Song

Department of Chemistry, Korea National University of Education, Chongwon, Chungbuk 363791, Korea

William L. Hase

Department of Chemistry and Biochemistry, Texas Tech University, Lubbock, Texas 79409

Scott L. Anderson*

Department of Chemistry, University of Utah, 315 S 1400 E, Salt Lake City, Utah 84112

Received: May 18, 2005; In Final Form: August 9, 2005

Quasiclassical, direct dynamics trajectories have been used to study the reaction of formaldehyde cation with molecular hydrogen, simulating the conditions in an experimental study of H_2CO^+ vibrational effects on this reaction. Effects of five different H_2CO^+ modes were probed, and we also examined different approaches to treating zero-point energy in quasiclassical trajectories. The calculated absolute cross-sections are in excellent agreement with experiments, and the results provide insight into the reaction mechanism, product scattering behavior, and energy disposal, and how they vary with impact parameter and reactant state. The reaction is sharply orientation-dependent, even at high collision energies, and both trajectories and experiment find that H_2CO^+ vibration inhibits reaction. On the other hand, the trajectories do not reproduce the anomalously strong effect of ν_2^+ (the CO stretch). The origin of the discrepancy and approaches for minimizing such problems in quasiclassical trajectories are discussed.

I. Introduction

Recently, we reported a detailed experimental study of the effects of collision energy (E_{col}) and reactant vibrational excitation on the reaction of H_2CO^+ with D_2.[1] Only one product channel, deuterium abstraction, was observed. For consistency with the experimental paper, we will use the generic label "hydrogen abstraction" (HA). Despite being exoergic by 0.20 eV, HA has an appearance energy of 0.4 eV, consistent with the energy of the lowest ab initio transition state (TS) on the reaction coordinate calculated in conjunction with the experiments. The reaction is dominated by a direct mechanism, and as expected for reaction over a substantial barrier, it is enhanced by collision energy. In contrast, the reaction is mode-specifically inhibited by H_2CO^+ vibration excitation. Most notably, excitation in the CO stretch mode, ν_2^+, results in roughly twice the inhibition that would be expected if the effect were proportional to vibrational energy. A similar pattern of vibrational effects is found over a wide range of collision energies, except very near the reaction threshold energy, where the cross-section depends only on total energy. One interesting point is that the pattern of H_2CO^+ vibrational effects is nearly identical to that observed over a wide collision energy range for the hydrogen abstraction reaction of H_2CO^+ with CD_4, despite the fact that the latter system is barrierless.[2] The similarity suggests that the factors

controlling HA in the two systems are similar and not strongly dependent on collision time scale or energy.

This paper reports a quasiclassical, direct dynamics trajectory study of $H_2CO^+ + D_2$ collisions at $E_{col} = 1.70$ eV, designed to allow detailed comparison with the experimental results. The goal was to gain additional insight into the reaction mechanism, including vibrational effects, and also to consider different approaches to treating vibrational dynamics with quasiclassical trajectories. The $H_2CO^+ + D_2$ system should be a good candidate for a quasiclassical direct dynamics study. The excited states of $H_2CO^+ + D_2$ are high enough in energy to rule out nonadiabatic behavior, allowing use of single reference quantum chemistry methods where the forces and Hessians can be evaluated analytically. With only two heavy atoms, it is feasible to run the thousands of trajectories needed to obtain good statistics for the different reactant vibrational states and to explore issues such as zero-point energy effects. Finally, because interesting effects are observed at high E_{col}, the calculations can be done in a regime where the energy and angular momenta are high enough that tunneling and rotational quantization effects should be negligible.

The most serious problem with the quasiclassical trajectory (QCT) method in this energy regime is the lack of vibrational quantization. Trajectories can transfer energy in and out of different modes in any amount, leading to several types of unphysical behavior. For example, the product vibrational distribution might have sub-quantum excitation in high-

Direct Dynamics Trajectory Studies

J. Phys. Chem. A, Vol. 109, No. 50, 2005 **11377**

frequency modes that would not be energetically accessible in reality. From the perspective of explaining vibrational effects on reactivity, early-time collision dynamics are most important, and here, the biggest question is how to deal with zero-point energy (ZPE). The QCT method attempts to simulate ZPE by adding half a quantum's worth of vibrational energy to each reactant mode; however, because vibrational motion is treated classically, this pseudo-ZPE can behave unphysically. In a real quantum system, a reaction can make use of only that fraction of ZPE associated with bonds being broken or with modes whose frequencies drop in the products or at the transition state. Conversely, the system has to come up with the energy required for the ZPE of any new bonds formed or of modes whose frequencies increase during reaction. In QCT, unphysical ZPE flow[3] can drive reactions, and products may be generated with vibrational energy below the ZPE. Aoiz et al. have identified lack of ZPE conservation at transition states as one of the major problems in the QCT method.[4] For our conditions, however, where the collision energy is much greater than the ZPE and TS energies, such effects are expected to be relatively minor.

Our previous QCT and experimental work on similar scattering systems, i.e., collisional excitation and collision-induced dissociation of $H_2CO^+ + Ne$,[5] and reaction of $H_2CO^+ + CD_4$,[6] suggests that quasiclassical trajectories accurately reproduce the experimental dynamics at high energies. Nonetheless, for this system, we have explored the effects of partially or entirely omitting ZPE from the reactants. In the final analysis, the best test is how well trajectories reproduce experiment. As shown below, the agreement is generally good, although there are interesting exceptions that provide some insight into the limitations of the methodology.

II. Computational Details

Quasi-classical, direct dynamics trajectories were calculated using the VENUS99 program of Hase and co-workers,[7] to set up the trajectory initial conditions, and the updating Hessian method of Schlegel and co-workers,[8] implemented in *GAUSSIAN 03*,[9] to propagate each trajectory. Because millions of ab initio force and Hessian evaluations are required, the level of ab initio theory used was necessarily modest. To select a suitable level of theory, we first performed relaxed potential energy surface (PES) scans for approach of D_2 to H_2CO^+ in several orientations with the candidate methods: MP2/6-311G** and B3LYP/6-311G**. We then compared these results to "benchmark" calculations, consisting of single-point calculations at the geometries sampled in the relaxed PES scans, using the MP2/aug-cc-pVTZ, QCISD(T)/cc-pVDZ, and CCSD(T)/cc-pVDZ levels of theory. For all methods, the $D_2-H_2CO^+$ surface has a broad, shallow (~50 meV), electrostatic well at long range (~2.9 Å center-of-mass separation), then a barrier peaking at ~1.5 Å center-of-mass separation, before dropping into a product-like H_2COD^+-D complex well. The benchmark calculations are in excellent agreement with G3 calculations done for stationary points on the PES, including the barrier and electrostatic H_2COD^+-D complex.[1] We note that the H_2COD^+-D complex is quite product-like and only bound by ~0.1 eV with respect to products. We expect, therefore, that the reaction cross-section and reactant vibrational effects should depend mostly on the dynamics for reactant approach and crossing the barrier to H_2COD^+-D formation. The MP2/6-311G** method was chosen for the trajectories, because it accurately tracks the QCISD(T) and CCSD(T) energy curves for reactant approach and yields a barrier only 0.02 eV below the benchmark value. In contrast, the B3LYP/6-311G** method yields a barrier 0.3 eV too low.

TABLE 1: Experimental and Calculated Reaction Energetics

reaction channels		expt[a] (eV)	MP2/6-311G** [c] (eV)
$H_2CO^+ + D_2$	→ $H_2COD^+ + D$	−0.20	−0.73 (−0.57)[d]
	→ $CH_2DO^+ + D$	3.43	3.27
	→ $HCOH^+ + D_2$	0.22	−0.09
	→ $D_2H^+ + HCO$	2.18	1.92
	→ CH_2DOD^+	−0.99	−1.24
	→ $CH_2OD_2^+$	−1.30	−1.89
	→ $HCO^+ + H + D_2$	1.09[b]	0.44

[a] Refs 18 and 19. [b] Refs 10−12. [c] Zero-point energy not included. [d] Zero-point energy included.

The experimental and MP2/6-311G** reaction energetics are listed in Table 1, including the complexes and several product channels not observed in the experiments. Note that the MP2/6-311G** method overestimates the exoergicity of the reaction as well as the depth of the H_2COD^+-D well. These errors appear to be a problem with the MP2 method, rather than the basis set, because the "benchmark" MP2/aug-cc-pVTZ calculation is even worse. This error is not a major problem here, because it should mainly affect the product recoil and internal energy distributions, which were not measured in the experiments. We expect that the trajectory results for the reaction cross-section and vibrational effects should be accurate, because the MP2 energetics for reactant approach and the rate-determining barrier are good. The MP2 method also significantly underestimates the H_2CO^+ dissociation energy (0.44 eV without ZPE, compared to 1.09 eV experimentally[10−12]), which has the effect of leading to collision-induced dissociation (CID − HCO^+ + H + D_2 products) in a small fraction of the trajectories.

The initial conditions for the trajectories were chosen to mimic the conditions of the experimental study. Because the experiment generated H_2CO^+ by resonance-enhanced multiphoton ionization of a supersonic molecular beam, a 50 K Boltzmann distribution was sampled to generate the H_2CO^+ initial rotational motion. For D_2, a rotation temperature of 300 K was used, because thermal D_2 was used in the scattering cell in the experiment. The initial reactant vibrational state was simulated by giving each atom momentum and displacement from equilibrium appropriate to the desired state, with random phases for the different modes. The main set of trajectories was run with both D_2 and H_2CO^+ having zero-point energy (ZPE), simulating reaction of ground-state reactants, and with H_2CO^+ having one additional quantum of excitation in ν_6^+(CH$_2$ in-plane rock), ν_4^+(CH$_2$ out-of-plane bend), ν_3^+(CH$_2$ scissors), ν_2^+(CO stretch), or ν_5^+(CH$_2$ asym stretch). The experimental and calculated energies of the H_2CO^+ vibrational states are listed in Table 2.

Randomly oriented H_2CO^+ and D_2 were given relative velocities corresponding to $E_{col} = 1.70$ eV, with an initial center-of-mass separation of 9.0 Å—well beyond the range of significant inter-reactant interaction. For each vibrational state, trajectories were run at 6 values of the impact parameter (b), ranging from 0.1 to 2.5 Å. At $b = 2.5$ Å, the angular deflection and energy transfer are already small, and no reactive trajectories were observed. The trajectory integration was performed with a step size of 0.25 amu$^{1/2}$ bohr (~0.7 fs), which gave conservation of total energy to better than 10^{-4} hartree. Trajectories were terminated when the center-of-mass distance between scattered products exceeded 10.0 Å. For the ground state and ν_2^+, 400 trajectories were run for each impact parameter. For other states, batches of 200 trajectories were run for each impact parameter. Trajectories took 2 to 3 h each on a 2.6 GHz pentium IV CPUs, and the complete set of ~9600

TABLE 2: Reactant Zero-Point Energies and H_2CO^+ Vibrational Modes and Energies

		experiment[b]		MP2/6-311G** [c]	
	type	E_{vib} (eV)	E_{vib} + ZPE (eV)	E_{vib} (eV)	E_{vib} + ZPE (eV)
D_2 (ground state)		0	0.185	0	0.199
H_2CO^+ (ground state)		0	0.612	0	0.675
H_2CO^+ (ν_6^+)	in-plane CH_2 rock	0.101	0.713	0.108	0.783
H_2CO^+ (ν_4^+)	out-of-plane CH_2 bend	0.114	0.726	0.139	0.813
H_2CO^+ (ν_3^+)	CH_2 scissors	0.143	0.755	0.163	0.838
H_2CO^+ (ν_2^+)	CO stretch	0.208	0.820	0.204	0.879
H_2CO^+ (ν_1^+)[a]	sym. CH_2 stretch	0.320	0.932	0.359	1.034
H_2CO^+ (ν_5^+)	asym.CH_2 stretch	0.337	0.949	0.377	1.052
H_2COD^+					1.034
transition state					0.936

[a] Not studied in the present work. [b] Refs 20−23. [c] The calculated ZPE and E_{vib} are not scaled.

trajectories required about $2^1/_2$ CPU years on a small dedicated Linux cluster.

Because vibrational motion is not quantized in quasiclassical trajectories, it is not clear how ZPE is best handled. The usual QCT approach is to simulate ZPE by adding appropriate amounts of vibrational motion to each mode, as was done in the main set of trajectories. The classical trajectories do not constrain this vibrational energy to remain correctly distributed as $^1/_2\hbar\omega$/mode. In particular, the formaldehyde ZPE amounts to 0.675 eV that can unphysically aid in surmounting the reaction barrier. To examine ZPE effects, another set of calculations was run, as above but with no reactant ZPE. Total omission of ZPE is also somewhat problematic, because in reality, the D_2 ZPE does become available as the barrier is surmounted (breaking the D−D bond), although this is presumably compensated to some degree by ZPE associated with the nascent OD bond. To test the effect of D_2 ZPE, we also ran a set of trajectories including ZPE only for the D_2 reactant. For this set, we only included trajectories for ground-state and ν_2^+-excited H_2CO^+.

For visualization of individual trajectories, we used the program gOpenMol.[13] Detailed analysis of individual trajectories and statistical analysis of the trajectory ensemble were done with programs written for this purpose. The kinetic energies (KEs) of relative motion (i.e., E_{col} and E_{recoil}) as well as the initial and final orbital angular momenta, are calculated straightforwardly from the center-of-mass velocities and impact parameters of reactants and products for each trajectory. The rotational angular momenta and rotational energies of the reactants and products are calculated as $\mathbf{J} = \mathbf{r} \times \mathbf{p}$, and $E_{rot} = (\mathbf{J}\cdot\omega)/2$, where ω is the angular velocity, determined as $\omega = \mathbf{J}\cdot\mathbf{I}^{-1}$, where $\mathbf{I}$ is the moment of inertia tensor. To approximately decouple the rotational and vibrational energies (i.e., to account for fluctuation of the classical E_{rot} resulting from vibration-induced changes in $\mathbf{I}$), E_{rot} is averaged over a time period corresponding to the final half-period of the lowest-frequency H_2CO^+ vibration. To calculate the vibrational energy (E_{vib}), we first calculate the total energy associated with nuclear motion of the reactants or products. This $E_{nuclear}$ includes both nuclear kinetic energy and that fraction of the instantaneous potential energy (PE) resulting from distortion away from the equilibrium geometry of the reactants or products. The vibrational energy is then determined by subtracting the KE of relative motion and the time-averaged E_{rot} from $E_{nuclear}$. The HA product scattering angle is given by $\theta_{scat} = \arccos[(\mathbf{v}_i\cdot\mathbf{v}_f)/(|\mathbf{v}_i||\mathbf{v}_f|)]$, i.e., the angle between the initial H_2CO^+ and final H_2COD^+ velocities, $\mathbf{v}_i$ and $\mathbf{v}_f$. Reaction cross-sections and average values of θ_{scat}, E_{col}, E_{recoil}, E_{rot}, and E_{vib} for the reactants (and products) are calculated as the usual b-weighted (and $P(b) \times b$-weighted) averages, as discussed below.

III. Results and Discussion

A. Nature of the Trajectories. Roughly 87% of all trajectories are characterized as direct, nonreactive scattering, resulting in conversion of varying fractions of the initial collision energy into product vibrational and rotational energies ($T \rightarrow E_{internal}$ conversion). The balance of the trajectories either represents the hydrogen abstraction channel (H_2COD^+ + D; 12%) or collision-induced dissociation (HCO^+ + H + D_2; 1%). In agreement with the experimental results, no trajectories are observed for H/D exchange or for production of $CH_2OD_2^+$, CH_2DOD^+, CH_2DO^+, or D_2H^+, reflecting the fact that these channels either involve high barriers or complicated rearrangements that are insignificant at high E_{col}.

As noted above, the 1% collision-induced dissociation (CID) branching is driven by the unphysically low MP2 dissociation energy for H_2CO^+—no CID is observed experimentally. In our previous study of H_2CO^+ CID in collisions with neon, we found that CID occurred exclusively in collisions where the Ne impacted on one of the H_2CO^+ H atoms.[5] Visualization of CID trajectories in this system shows the same propensity for D_2-on-H collisions. Furthermore, the CID mechanism is sequential, i.e., collision activation of H_2CO^+ and D_2, followed by the dissociation of excited H_2CO^+ as follows

$$H_2CO^+ + D_2 \rightarrow H_2CO^+ (E_{H_2CO^+}) + D_2 (E_{D_2}) \rightarrow$$
$$HCO^+ (E_{HCO^+}) + H + D_2 (E_{D_2})$$
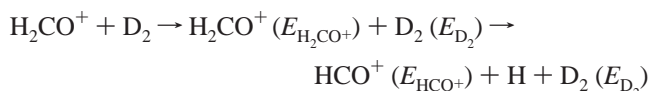
where $E_{H_2CO^+}$, E_{D_2}, and E_{HCO^+} are the internal energies of the indicated species. Such collisions are mechanistically distinct from the concerted, "D_2-on-O" collisions leading to HA; therefore, we conclude that the spurious CID channel does not affect the HA cross-sections. Rather, CID simply represents the fraction of nonreactive collisions where $E_{H_2CO^+}$ is high enough to cause dissociation on the trajectory time scale. These trajectories are, therefore, counted as nonreactive, and $E_{H_2CO^+}$ is calculated as the sum of E_{HCO^+}, the MP2 CID threshold energy, and the relative kinetic energy of the HCO^+ − H fragments.

A typical HA trajectory is illustrated in the bottom frame of Figure 1, where rDD and rOD are the bond length of D_2 and the distance from the abstracted D atom to the oxygen atom of H_2CO^+, respectively. The HA trajectories are direct at E_{col} = 1.70 eV, with only one turning point in the relative motion of the reactant centers of mass. The time during which H_2CO^+ and D_2 are interacting strongly is 20−40 fs as shown by the potential energy changes during the trajectory (top frame). This time scale is comparable to the periods of the lower-frequency H_2CO^+ vibrations (ν_6^+, ν_4^+, and ν_3^+) and longer than those of

Direct Dynamics Trajectory Studies
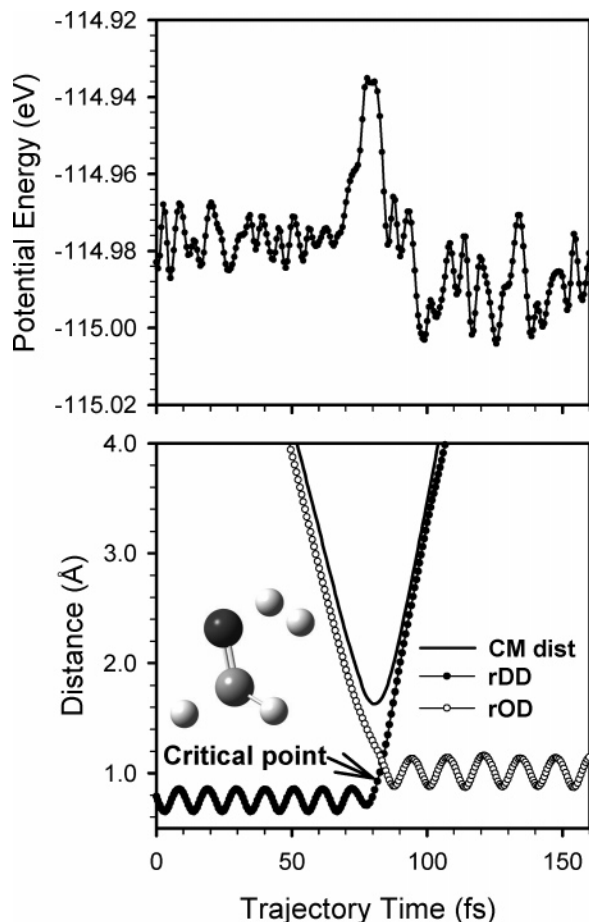
J. Phys. Chem. A, Vol. 109, No. 50, 2005 **11379**

Figure 1. A representative plot of HA trajectories: (top) the variation of potential energy during trajectory and (bottom) the variation of rDD (D_2 bond length), rOD (separation of the abstracted D atom from the formaldehyde oxygen atom), and center-of-mass reactant/product distance during trajectory.

ν_2^+ and ν_5^+. The direct reaction mechanism observed in trajectories is consistent with our experimental paper, where we inferred, on the basis of the comparison of measured and RRKM reaction efficiencies, that the HA reaction is direct at all energies except possibly at the reaction threshold.

B. Comparison with Experiment. We start by comparing trajectory results with experimental observables, because the trajectories are only useful if they are accurate. In the experiment, the heavy ion−light neutral kinematics preclude extracting recoil velocity and angular distribution information; therefore, the only observable is the reaction integral cross-sections, given in Figure 2 and Table 3. The trajectory HA cross-section, σ_{HA}, is calculated using an extended closed trapezoidal approximation[14] to the usual integral form

$$\sigma_{HA} = 2\pi \int_0^{b_{max}} P(b) \times b \cdot db \approx$$
$$\pi \sum_{b_i=0}^{b_{max}} [P(b_i) \times b_i + P(b_{i+1}) \times b_{i+1}] \times (b_{i+1} - b_i) \quad (1)$$

where b_{max} is the maximum b at which reaction is observed, and $P(b)$ is the HA opacity function, i.e., the fraction of reactive trajectories at each impact parameter.

The agreement between calculated and experimental cross-sections is quite good, considering that there are no adjustable parameters. For the main trajectory set with full ZPE, the absolute agreement $(\sigma_{expt} - \sigma_{traj})/\sigma_{expt}$ is within 11% for all states
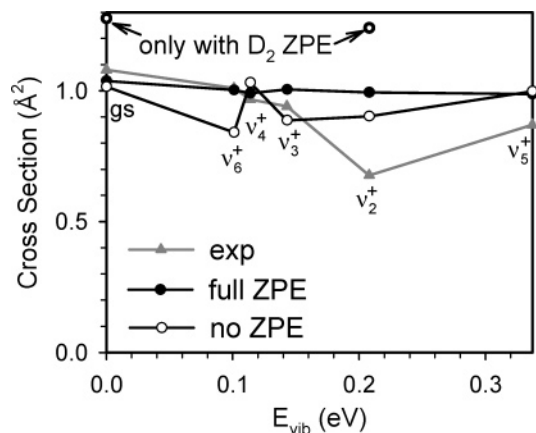

Figure 2. Comparisons of trajectory and experimental HA cross-sections for different vibrational states at $E_{col} = 1.70$ eV.

except ν_2^+, and both experiment and trajectories show a modest inhibition of HA with formaldehyde vibrational excitation. This suggests that the trajectories do a reasonable job of capturing the rate-limiting dynamics.

The question is whether any significance should be attached to fact that the trajectories predict less variation in cross-section with reactant vibrational mode than is observed experimentally, given the absolute uncertainties listed in the table. Both the experimental and trajectory studies were designed to minimize the relative error in comparing vibrational effects. The experimental absolute uncertainty reflects factors such as uncertainties in the target gas pressure profile and relative collection efficiency for reactant and product ions. These factors cancel in calculations of vibrational effects $(\sigma_\nu/\sigma_{ground\ state})$, and the resulting relative uncertainty is estimated to be only ~10%. For the trajectories, the absolute uncertainties reflect the limited number of trajectories (1200−2400) run for each state. To minimize relative error, each set of trajectories was run with the same initial random number seed. As a consequence, all vibrational states used the same set of pseudo-random initial conditions (orientation, rotational energy, ...), with the obvious exception that the mode of vibrational excitation varied. Therefore, we expect that errors resulting from inadequate sampling of initial conditions should, to a large extent, cancel in comparing results for the different reactant states. For the ground state and for ν_2^+, where the experiments show the largest effects, we ran additional trajectory sets, bringing the statistical uncertainty down to ~13%. Therefore, the $\sigma_{\nu_2^+}/\sigma_{ground\ state}$ ratio is outside the combined experimental and trajectory relative uncertainties. Furthermore, the $\sigma_{\nu_2^+}/\sigma_{ground\ state}$ ratios calculated from the two sets of trajectories (with different random seeds) differ by only ~2%−far less than the ~13% statistical uncertainty. This close agreement suggests that there is, indeed, significant cancellation of error in ratios of trajectory results calculated with identical random seeds.

In addition to comparing experimental and trajectory cross-sections, Table 3 presents the mean product recoil energy, $\langle E_{recoil}\rangle$, vibrational energy, $\langle E_{vib}'\rangle$, rotational energy, $\langle E_{rot}'\rangle$, and scattering angle $\langle \theta_{scat}\rangle$. All calculated values in Table 3 are from the trajectory set with ZPE included. The cross-sections are reported with the usual statistical uncertainties, as discussed above. For $\langle E_{recoil}\rangle$, $\langle E_{vib}'\rangle$, $\langle E_{rot}'\rangle$, and $\langle \theta_{scat}\rangle$, the "uncertainties" are actually the widths (at half-maximum) of these energy and θ_{scat} distributions. The opacity functions, $P(b)$, are given in Figure 3 for different H_2CO^+ vibrational states, along with the corresponding b-weighted opacity functions $P(b) \times b$, which describe the contribution of each b range to the cross-section

TABLE 3: Comparison of Trajectory and Experimental Results for the Hydrogen Abstraction Reaction[a]

	experimental	trajectory				
	σ_{HA} (Å^2)	σ_{HA} (Å^2)	$\langle E_{recoil} \rangle$ (eV)	$\langle E_{vib}' \rangle$ (eV)	$\langle E_{rot}' \rangle$ (eV)	$\langle \theta_{scat} \rangle$ (deg)
ground state	1.08 ± 0.2	1.04 ± 0.13 $(1.01 \pm 0.30)^b$	0.95 ± 0.32 (0.99 ± 0.21)	2.12 ± 0.34 (1.21 ± 0.18)	0.26 ± 0.12 (0.27 ± 0.11)	116 ± 19 (103 ± 14)
ν_6^+	1.01 ± 0.2	1.00 ± 0.26 (0.84 ± 0.28)	0.93 ± 0.32 (0.94 ± 0.19)	2.26 ± 0.33 (1.35 ± 0.17)	0.25 ± 0.11 (0.28 ± 0.11)	118 ± 18 (103 ± 14)
ν_4^+	0.97 ± 0.2	0.99 ± 0.26 (1.03 ± 0.30)	0.94 ± 0.30 (0.95 ± 0.20)	2.29 ± 0.32 (1.38 ± 0.19)	0.24 ± 0.12 (0.26 ± 0.10)	118 ± 19 (101 ± 13)
ν_3^+	0.94 ± 0.2	1.00 ± 0.26 (0.89 ± 0.26)	0.91 ± 0.29 (0.96 ± 0.20)	2.33 ± 0.32 (1.42 ± 0.20)	0.25 ± 0.13 (0.25 ± 0.09)	118 ± 20 (103 ± 15)
ν_2^+	0.68 ± 0.2	0.99 ± 0.13 (0.90 ± 0.28)	0.96 ± 0.33 (1.02 ± 0.20)	2.33 ± 0.36 (1.40 ± 0.19)	0.25 ± 0.12 (0.25 ± 0.10)	117 ± 19 (105 ± 16)
ν_5^+	0.88 ± 0.2	0.98 ± 0.26 (1.00 ± 0.30)	0.92 ± 0.33 (0.94 ± 0.19)	2.56 ± 0.33 (1.64 ± 0.19)	0.23 ± 0.11 (0.26 ± 0.09)	116 ± 19 (99 ± 15)

^{a} Trajectory results were obtained with ZPE included in both reactants. ^{b}The values in parentheses are calculated from trajectories with no reactant ZPE.
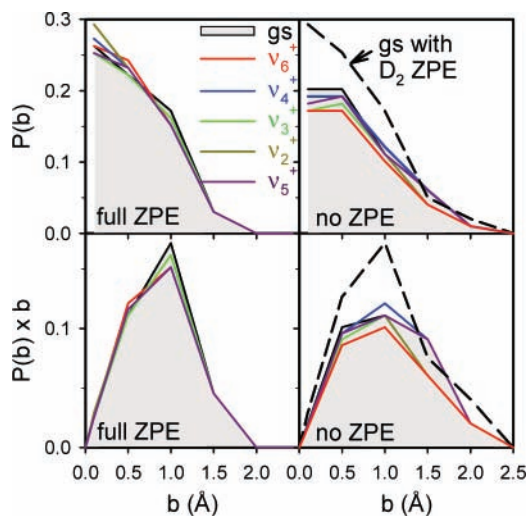

Figure 3. HA opacity functions for different vibrational states at E_{col} = 1.70 eV, with or without ZPE in reactants.

Figure 4. Computed center-of-mass H_2COD^+ velocity contour maps: (top) with reactant ZPE and (b) without reactant ZPE. The labels on the map show the major contributing b at each corresponding angle.

(eq 1). The left and right columns correspond to trajectory results obtained with and without reactant ZPE, respectively. The effects for ground-state reactants of including only D$_2$ ZPE are shown with dashed lines.

Figure 4 reports the calculated H_2COD^+ recoil velocity maps for reactants with and without ZPE. Scales are given both for Cartesian (i.e., axial and radial) velocities and for recoil angle and speed, in both cases referenced to the relative velocity axis. The maps are simply the $P(b) \times b$-weighted sum of the product ion recoil velocity distributions obtained for the sets of trajectories calculated at b = 0.1, 0.5, 1.0, 1.5, and 2.0 Å. The peak recoil velocity for each impact parameter is indicated by the "$b = n.m$" labels, and only b values with reactive trajectories are shown. As expected, the peak scattering angle decreases with increasing b, and the resulting $\langle \theta_{scat} \rangle$ is ~110° with associated recoil speed peaking at 550 m/s (top frame). The calculated recoil velocities are probably somewhat excessive, because the exoergicity is overestimated in the MP2 calculations. Also shown in the bottom frame of Figure 4 is the H_2COD^+ velocity map calculated from trajectories without reactant ZPE. ZPE effects will be discussed below.

C. The HA Reaction Mechanism.

1. Effects of Impact Parameter. From eq 1, it can be seen that the magnitude of σ_{HA} is determined by how $P(b)$ varies with b. For example, the line-of-centers (LOC) model, which is commonly used to fit the energy dependence of reactions with activation energies, predicts that $P(b)$ is unity up to a b_{max}
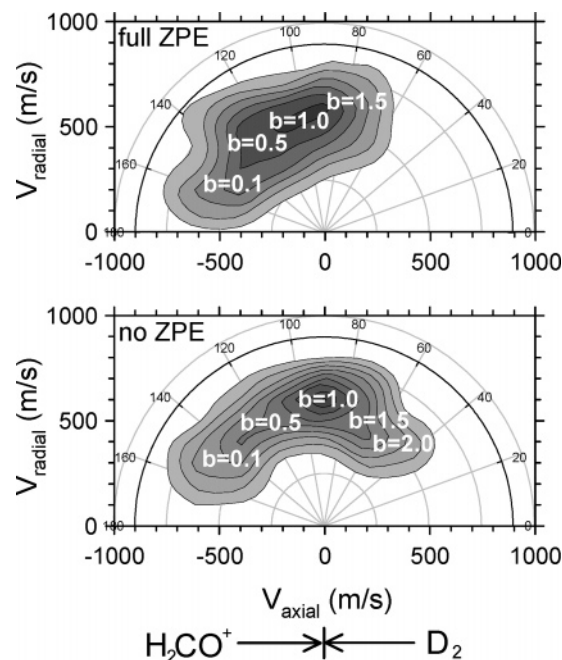
determined by the requirement that the energy along the line-of-centers (E_{LOC}) must exceed the barrier height.[15] For this system, the orientation-averaged hard sphere radius is ~2.2 Å, and for E_{col} = 1.7 eV and a 0.4 eV barrier, b_{max} would be ~1.7 Å in the LOC model, in reasonable agreement with the maximum b where reactive trajectories are observed. On the other hand, the trajectory $P(b)$'s never approach unity and fall off gradually with increasing b, rather than having a sharp b_{max} cutoff. As a consequence, σ_{HA} is almost an order of magnitude smaller than the LOC estimate. The b dependence is somewhat different for trajectories with and without ZPE, and ZPE effects will be discussed below. The lower frames of Figure 3 show the b-weighted opacity functions, i.e., the contribution of each range of b to the total cross-section. With or without ZPE, the intermediate range of b (=0.5−1.5 Å) dominates the cross-section, leading to strong sideways scattering (Figure 4).

The effects of H_2CO^+ vibrational state on $P(b)$ depend on whether ZPE is included. With full ZPE, H_2CO^+ vibrational effects are small. $P(b)$ increases slightly for $b \leq 0.5$ Å and decreases slightly for $b \approx 1$ Å. The $P(b) \times b$ distribution is dominated by intermediate impact parameters, leading to a slight
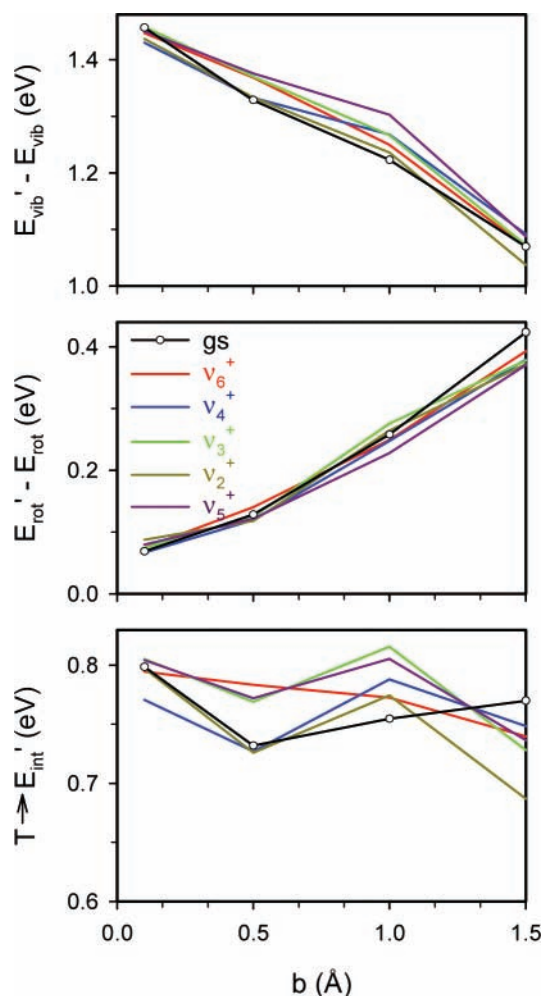
Direct Dynamics Trajectory Studies

J. Phys. Chem. A, Vol. 109, No. 50, 2005 **11381**

Figure 5. Mean increase in HA products vibrational and rotational energies, and net translational-to-internal ($T \rightarrow E_{int}'$) energy transfer vs impact parameter for different vibrational states.

vibrational inhibition of σ_{HA}. For trajectories without ZPE, vibrational effects are larger, consisting of inhibition at all b.

We also investigated product energy partitioning associated with the HA reaction. The top frame of Figure 5 shows the *net increase* in vibrational energy, i.e., the average product E_{vib}' minus the reactant E_{vib} ($\langle E_{vib}' \rangle - E_{vib}$, including ZPE; see Table 2). The middle frame gives the net increase in rotational energy: $\langle E_{rot}' \rangle - \langle E_{rot} \rangle$ ($\langle E_{rot} \rangle = 0.03$ eV). Both forms of internal energy increase in the products—not unexpected for an exoergic reaction at high E_{col}. The net increase in $\langle E_{vib}' \rangle$ decreases with increasing b, presumably because large b collisions have more energy tied up in orbital motion and less along the line-of-centers, where it can drive impulsive $T \rightarrow E_{vib}'$ conversion. For space reasons, we show only the average product E_{vib}'; however, we have also examined the distributions of E_{vib}' as a function of b for different reactant states. These distributions are not particularly informative; however, they do show that unphysical collisions with E_{vib}' less than the ZPE are insignificant.

As expected, the net increase in $\langle E_{rot}' \rangle$ (middle frame) increases with increasing b, reflecting the larger orbital angular momentum and longer moment arm. Because this reaction results in recoil of a light, atomic product, we considered the possibility that the final E_{rot}' might be constrained by angular momentum conservation. This does not appear to be the case.

The bottom frame of Figure 5 shows the translational endoergicity, i.e., the net conversion of translational energy (T) to product internal energy (E_{int}'). The net $T \rightarrow E_{int}'$ conversion

is roughly independent of impact parameter, reflecting the fact that $T \rightarrow E_{vib}'$ and $T \rightarrow E_{rot}'$ conversion processes have opposite dependence on b. The reactive collisions convert ~44% of the collision energy to product internal energy.

One counterintuitive point shown in the top and bottom frames of Figure 5 is that reactant vibrational excitation enhances net $T \rightarrow E_{vib}'$ conversion. The net increase in E_{vib} during a collision can be thought of as a competition between $T \rightarrow V$ processes that tend to increase product E_{vib}', and $V \rightarrow T$ and $V \rightarrow R$ processes that tend to reduce the net vibrational excitation. At high E_{col}, the $T \rightarrow V$ process dominates; thus, E_{vib}' is substantially higher than the reactant E_{vib} for all states. On the other hand, intuition suggests that, as the reactant E_{vib} increases, $V \rightarrow T$ and $V \rightarrow R$ processes should become more important, thus the *net increase* in E_{vib}' become smaller. Just such behavior was observed in previous trajectory studies of $H_2CO^+ + Ne$[5] and $H_2CO^+ + CD_4$ collisions. In the $H_2CO^+ + D_2$ HA reaction, the presence of initial vibrational excitation enhances the $T \rightarrow V$ process more than enough to compensate for $V \rightarrow T$ or $V \rightarrow R$ conversion. This counterintuitive behavior is observed only for the reactive collisions—nonreactive trajectories show the expected decrease in net $T \rightarrow V$ conversion with increasing reactant E_{vib}. The interesting point here is that, while H_2CO^+ vibrational excitation inhibits reaction (Figure 2), for those collisions that do react, the reactant vibrational excitation leads to an increase in net $T \rightarrow V$ conversion.

2. Dependence on Collision Orientation. Perhaps the most obvious feature of this reaction is that the efficiency is quite low, even for energies well above the activation barrier. In the experimental paper,[1] we pointed out that the transition state is orientationally tight, i.e., calculation of the potential surface near the TS showed that the 0.4 eV activation barrier is quite dependent on orientation. On the other hand, the 1.7 eV collision energy studied here is well above the barrier height in almost any orientation; thus, we might expect that orientation should be less important.

To quantify the dependence of reactivity on geometric parameters such as orientation, we need to define a "critical point" in each trajectory where the parameters are recorded. Here, we take the critical point to be the first time step where two conditions are satisfied simultaneously (see Figure 1): the D–D bond length exceeds 0.88 Å (~$1.2 \cdot R_e(D_2)$), and the O–D distance of the nascent OD bond is less than 1.40 Å ($R(OD)$ in the H_2COD^+ product is 1.0 Å). Trajectory visualization suggests that this condition serves as a reasonable definition of the dividing surface between reactant and products. Trajectories reaching this point always dissociate to products, but if a point significantly earlier on the reaction coordinate is used, some nonreactive trajectories are included. It should be noted that this critical point definition is quite reactant-like, consistent with the fact that the ab initio transition state for the HA reaction is also reactant-like.[1] For nonreactive trajectories, which never reach this critical point, we characterize the collision geometry at the point of closest approach of the H_2CO^+ O atom to one of the D atoms of D_2, i.e., the closest approach to a geometry where D transfer might occur. In both reactive and nonreactive collisions, the critical point occurs within ~5 fs of the maximum in the potential energy (Figure 1).

In thinking about the orientation effects, three angles appear most likely to be important: α_{D-O-C}, the angle between the CO bond axis and the D atom that will be abstracted; Φ_{plane}, the dihedral angle that the abstracted D atom makes with respect to the H_2CO^+ equilibrium plane; α_{D-D-O}, the angle between the D_2 bond axis and the O atom. Figure 6 shows the reaction
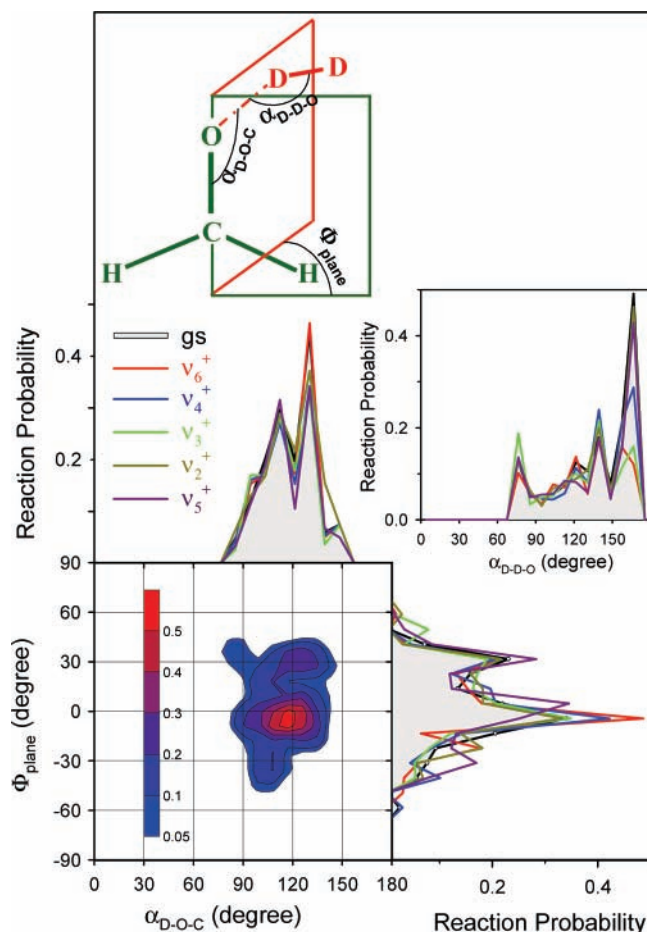
Figure 6. Dependence of reaction probability on α_{D-O-C}, Φ_{plane}, and α_{D-D-O}; the contour map is for the ground state only. The inserted sketch shows the definition of various angles.

probability (fraction of reactive trajectories) as a function of these angles. The dependence on each angle is shown for all H_2CO^+ reactant states, and the contour map shows the combined dependence on α_{D-O-C} and Φ_{plane} for reaction of the ground state. Positive and negative Φ_{plane} angles correspond to approach to the instantaneously convex and concave faces of the vibrating H_2CO^+, respectively. The key point is that reactivity depends strongly on all three orientation angles, which clearly is a reasonable explanation for the observed low reaction efficiency. The maximum reaction probability (~ 0.5) occurs in collisions where D_2 approaches with one D atom in the H_2CO^+ plane and with α_{D-O-C} near 120°, which is close to the corresponding angle in the H_2COD^+ product. Peak reaction probability also requires linear α_{D-D-O} (the apparent peaking at $\sim 170°$ simply reflects the histogramming scheme). The smaller peak at $\alpha_{D-D-O} \approx 80°$ is a consequence of the fact that both OD distances are nearly equal in such geometries, roughly doubling the probability that one D will be abstracted.

The contribution each range of angle makes to the HA cross-section depends on the reaction probability versus angle (Figure 6), but also on the probability of colliding in a particular orientation (the orientation distribution). The orientation distribution is independent of Φ_{plane}, i.e., there is no weighting effect for the dihedral angle. The orientation distribution is proportional to $\sin(\alpha_{D-O-C})$, shifting the weighted reaction probability so that it peaks at $\alpha_{D-O-C} \approx 110°$. The weighting for α_{D-D-O} also, in principle, varies like $\sin(\alpha_{D-D-O})$; however, the situation is complicated by indistinguishability of the D atoms and our definition of the angle as "O atom—closest D atom—farthest D

atom". The probability of having collisions with $\alpha_{D-D-O} < 90°$ is thereby reduced, reaching zero at $\sim 70°$. The resulting weighted reaction probability is broadly peaked about $\alpha_{D-D-O} \approx 110°$, and the small peak at $\sim 80°$ (Figure 6) is suppressed.

The moments of inertia for D_2 rotation and for rotation of H_2CO^+ about its symmetry axis are low. In such cases, we might expect that the dependence of the barrier energy on angle[1] might lead to orientational steering during reactant approach. Note, however, that the reduced mass for the reactant approach is also low, so that the collision time is quite short at $E_{col} = 1.7$ eV (Figure 1). If orientation steering were significant, it would be evident in the form of nonstatistical distributions of the orientation angles at the critical point. Within the uncertainty, the distributions are all statistical, i.e., there is no orientational steering.

Taken together, the experimental and trajectory results suggest the following mechanism. The lack of vibrational enhancement of HA probability indicates that barrier crossing is driven only by collision energy. The fact that the $P(b)$ distributions go to zero near the b value predicted from the LOC model suggests, further, that it is the line-of-centers projection of E_{col} that is important. On the other hand, the trajectory $P(b)$ functions differ from the LOC model prediction in having smaller peak magnitudes and in decreasing smoothly with b, rather than having a sharp cutoff. The small peak magnitudes can clearly be explained by the strong orientation sensitivity, leading us to wonder if orientation also accounts for the b dependence of $P(b)$. Specifically, might the falloff in $P(b)$ result from tightening of the orientation requirements with increasing b? Figure 7 shows that this is the case, i.e., the reactive angular range narrows for all three orientation angles with increasing b. Such behavior makes sense. The orientation dependence derives from the fact that the barrier energy increases as the orientation deviates from the ideal geometry. The energy available to drive barrier crossing, which for this system appears to be the LOC energy, decreases with increasing b; thus, reaction increasingly occurs only in near-ideal orientations.

3. Effects of ZPE. The results and discussion presented so far are mostly based on the analysis of trajectory results with ZPE included for both reactants. Given the concerns regarding unphysical ZPE effects in quasiclassical trajectories,[1,16,17] and our interest in reactant vibrational effects, it is interesting to try to understand the effects of ZPE. As noted, a second set of trajectories was calculated with no reactant ZPE, and a more limited set (ground state and ν_2^+ only) was done with only D_2 having ZPE.

Adding vibrational energy to simulate reactant ZPE has several effects, as shown in Figure 3. Including ZPE increases $P(b)$ for low b but also causes a compensating decrease in the maximum b leading to reaction. As a result, the shape of the b-weighted opacity function is sensitive to ZPE (lower frames), but the cross-section in Figure 2, i.e., the integral of $P(b) \times b$, is nearly unaffected. Closer examination shows that this ZPE independence of σ_{HA} is the result of compensating effects from H_2CO^+ and D_2 ZPE. Comparison of the "D_2 ZPE" and "no ZPE" results in Figure 3 shows that D_2 ZPE enhances reaction at low b with little effect on high b collisions. Comparison of the D_2 ZPE and full ZPE results shows that H_2CO^+ ZPE decreases reactivity at all b, however, because the cross-section depends on $P(b) \times b$; the dominant effect is decreasing reactivity at large b. While these effects largely cancel in the cross-section, the shift to larger impact parameters when ZPE is omitted does lead to a broader and less backscattered angular distribution
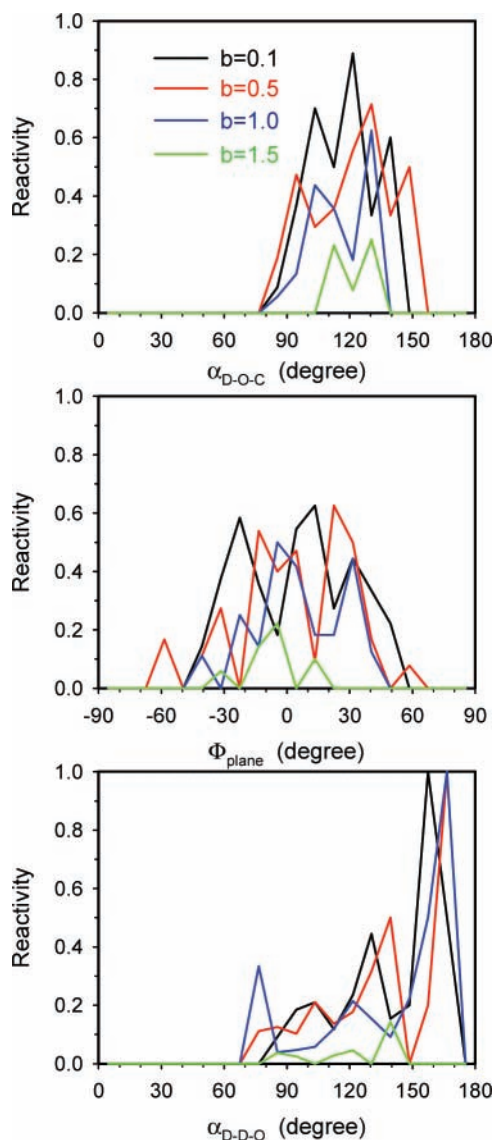
Direct Dynamics Trajectory Studies

J. Phys. Chem. A, Vol. 109, No. 50, 2005 **11383**

Figure 7. Dependence of the ground-state reaction probability on α_{D-O-C}, Φ_{plane}, and α_{D-D-O}, for different impact parameters.

(Figure 4). Unfortunately, the kinematics for this system do not allow us to measure the angular distribution for comparison.

It might be expected that the presence of ZPE could influence collisional energy transfer, because nothing in the quasiclassical method prevents conversion of ZPE into other forms of energy. Such effects turn out to be small for our high E_{col}, apparently because the short collision time does not provide sufficient time for unphysical flow of ZPE. Plots such as those in Figure 5 for the "no ZPE" trajectories are essentially identical to those in Figure 5, with the exception of one subtle effect. The presence of ZPE slightly increases the amount of net $T \rightarrow V$ energy transfer in the HA reaction. This effect is consistent with the observation that exciting the various vibrational modes also increases the net $T \rightarrow V$ conversion in reactive collisions, discussed above.

The effects of ZPE on the orientation dependence of the reaction probability are more interesting. An analysis analogous to that in Figure 6 indicates that reactant ZPE does change the patterns of reaction probability versus α_{D-O-C}, α_{D-D-O}, and Φ_{plane}. For α_{D-O-C} and Φ_{plane}, omitting ZPE shifts the angles of peak reactivity from 130° to 120° for α_{D-O-C} and from 0° to −30° for Φ_{plane}, but without changing the width of the reaction probability distributions. For α_{D-D-O}, on the other hand,

omitting ZPE eliminates the peak at $\alpha_{D-D-O} = 70-80°$ shown in Figure 6, i.e., reaction is less dependent on DDO angle for collisions with ZPE. This effect results entirely from the D_2 ZPE, i.e., D_2 with some vibrational excitation can transfer a D atom over a wider range of orientation angles. Nonetheless, because the probability of colliding in this 70−80° orientation range is small, the net effect on cross-section is negligible.

As indicated in Figures 2 and 3, adding only D_2 ZPE does have a significant effect, increasing the cross-section by increasing $P(b)$ at small b, without affecting reactivity at large b. Enhancement by D_2 ZPE is not surprising, given that the reaction coordinate has a large component of D_2 stretching motion, with the D_2 bond elongated ∼10% in the transition state structure. On the other hand, as noted above, H_2CO^+ ZPE inhibits the HA reaction both by decreasing the magnitude of $P(b)$ and by decreasing the maximum b where reaction occurs. Because the H_2CO^+ ZPE is distributed over six degrees of freedom, the origin of the effect is complicated, as discussed in the next section.

4. Vibrational Inhibition. The remaining question is how the H_2CO^+ vibrations affect the HA reaction. Both trajectories and experiment find that H_2CO^+ vibrational excitation inhibits the reaction, although the trajectories predict much weaker effects (Figure 2). Inhibition from H_2CO^+ vibration can also be inferred by comparing the D_2 ZPE and full ZPE results, which indicate that inclusion of 0.675 eV of H_2CO^+ ZPE motion results in a 20% inhibition. On the other hand, the trajectories did not recover the ∼30% mode-specific inhibition from ν_2^+ excitation observed experimentally. This raises questions regarding the usefulness of quasiclassical dynamics to describing vibrational effects, particularly relatively small mode-specific effects in polyatomic molecules. We note that, for the similar hydrogen abstraction reaction of H_2CO^+ with CD_4, trajectories accurately reproduced the substantial enhancement from CD_4 distortion vibration,[1] but also predicted small enhancements from various H_2CO^+ modes, whereas experiment shows 15−30% inhibitions from H_2CO^+ excitation. On the other hand, in a study of $T \rightarrow V$ energy transfer in collisions of mode-selectively excited H_2-CO^+ with Ne, the trajectory results agreed quantitatively with experiment, even for subtle mode-specific behavior.[5] In both these previous studies, only trajectories with full ZPE were studied.

There are a number of reasons why quasiclassical trajectories might fail for this kind of problem. The vibrational initial states are prepared on the basis of normal coordinates; thus, anharmonicity could potentially mix the initially excited mode during the reactant approach. Such mixing seems unlikely in this case, because the time from trajectory initiation to collision is only a few vibrational periods. Nonetheless, we looked for mode scrambling by running trajectories for particular reactant states (without ZPE) at 5 Å impact parameter, where collisional mixing is negligible. On a time scale much longer than that relevant here, there is no significant change in the character of the vibrational motion.

A more significant effect may be coupling of the desired vibrational motion with motions added to simulate ZPE. Because vibration is not quantized, it is possible for zero-point motion to transfer between modes (because of anharmonic coupling), which could result in ZPE "pooling" into particular modes[17] or exchange with the excited mode. Again, we attempted to address this issue by visualizing large b collisions, as above, but with ZPE in the initial conditions. Plots of various bond angles and lengths versus time show the expected multimode beating patterns; however, there is no evidence of dephasing or changes

in amplitude over time, at least for the few hundred femtosecond time period of interest for the reactant approach.

We also considered the possibility that, for this reaction, the motions from ZPE were simply washing out the effects of specific modes. This idea was tested by running trajectories without ZPE and with ZPE only in D_2. As shown in Figure 2, complete omission of ZPE does result in larger calculated vibrational inhibitions, in better overall agreement with experiment, but still does not reproduce the anomalously large effect of ν_2^+. Similarly, for trajectories with D_2 ZPE only, only a small inhibition from ν_2^+ excitation was found.

In the experimental study, the only obvious trend in vibrational mode effects was that modes involving CO stretching caused larger inhibitions than would be expected from their energies, particularly at low E_{col}, where vibrational effects are generally larger than at $E_{col} = 1.7$ eV. Normal modes with substantial CO stretch motion are ν_2^+, the CO stretch, ν_6^+, the CH_2 in-plane rock, and ν_3^+, the CH_2 scissors mode. Only ν_2^+ still has an anomalously large effect at high E_{col}, presumably because this mode has the highest energy and largest amplitude CO stretching component of the three modes. In the experimental paper, we speculated that the inhibiting effect of these H_2CO^+ vibrations might result from a vibration-induced tightening of the orientation restrictions associated with the HA reaction. In particular, we showed that compressing the CO bond to its classical turning point in the ν_2^+ vibration resulted in significantly sharper dependence of the activation energy on α_{D-O-C}. The interaction potential used to support that explanation was calculated at the same level of theory that was used in the trajectories.

If this were the mechanism for the vibrational inhibition, Figure 6 would show narrower distributions of reaction probability versus α_{D-O-C} for vibrationally excited reactants. No such sharpening is observed, although this may simply reflect the fact that the vibrational effects on the trajectories are unphysically small. Note, however, that in Figure 2, the effects of ν_2^+, ν_3^+, and ν_6^+ are larger for the trajectories with no ZPE. Therefore, we also examined reaction probability versus α_{D-O-C} for the trajectories with no ZPE. Here, the effects of vibration are clearer; however, what we see is that ν_2^+ excitation reduces reaction probability across the entire range of reactive orientations, rather than narrowing the reactive angular range. The phenomenon that vibration changes reactivity, rather than changing the range of reactive orientations, was also observed in the hydrogen abstraction reaction of H_2CO^+ with CD_4.[2,6] In that system, the HA reaction is activationless but inefficient because of a strong dependence on reactant orientation. The CD_4 distortion mode of interest in our trajectory study strongly *enhances* the HA reaction; nonetheless, the trajectories indicated no change in the range of reactive orientations.

IV. Conclusions

Direct dynamics trajectories adequately reproduce the main features of the hydrogen abstraction reaction of H_2CO^+ with D_2, including the magnitude of the absolute cross-section and the general trend of vibrational inhibition. The low reaction efficiency is shown to be the result of strong sensitivity to three orientation angles, and it was further shown that the orientation sensitivity sharpens with increasing impact parameter. It appears that a combination of a line-of-centers model for the energetics,

with the *b*-dependent orientation sensitivity, can explain most of the experimental observations.

The trajectories correctly indicate that H_2CO^+ vibrational excitation inhibits reaction, but they do not correctly reproduce the experimental effect of ν_2^+ excitation. Omitting simulated ZPE from the quasiclassical initial conditions increases the sensitivity to reactant vibrational excitation, but still does not reproduce the magnitude of the ν_2^+ effect.

References and Notes

(1) Liu, J.; Anderson, S. L. *J. Chem. Phys.* **2004**, *120*, 8528.

(2) Liu, J.; Devener, B. V.; Anderson, S. L. *J. Chem. Phys.* **2003**, *119*, 200.

(3) Swamy, K. N.; Hase, W. L. *J. Phys. Chem.* **1983**, *87*, 4715.

(4) Aoiz, F. J.; Banares, L.; Herrero, V. J. *J. Chem. Soc., Faraday Trans.* **1998**, *94*, 2483.

(5) Liu, J.; Song, K.; Hase, W. L.; Anderson, S. L. *J. Chem. Phys* **2003**, *119*, 3040.

(6) Liu, J.; Song, K.; Hase, W. L.; Anderson, S. L. *J. Am. Chem. Soc.* **2004**, *126*, 8602.

(7) Hase, W. L.; Bolton, K.; de Sainte Claire, P.; Duchovic, R. J.; Hu, X.; Komornicki, A.; Li, G.; Lim, K.; Lu, D.; Peslherbe, G. H.; Song, K.; Swamy, K. N.; Vande Linde, S. R.; Varandas, A.; Wang, H.; Wolf, R. J. VENUS99: A general chemical dynamics computer program, 1999.

(8) Bakken, V.; Millam, J. M.; Schlegel, H. B. *J. Chem. Phys.* **1999**, *111*, 8773.

(9) Frisch, M. J.; Trucks, G. W.; Schlegel, H. B.; Scuseria, G. E.; Robb, M. A.; Cheeseman, J. R.; J. A. Montgomery, J.; Vreven, T.; Kudin, K. N.; Burant, J. C.; Millam, J. M.; Iyengar, S. S.; Tomasi, J.; Barone, V.; Mennucci, B.; Cossi, M.; Scalmani, G.; Rega, N.; Petersson, G. A.; Nakatsuji, H.; Hada, M.; Ehara, M.; Toyota, K.; Fukuda, R.; Hasegawa, J.; Ishida, M.; Nakajima, T.; Honda, Y.; O. Kitao; Nakai, H.; Klene, M.; Li, X.; Knox, J. E.; Hratchian, H. P.; Cross, J. B.; Adamo, C.; Jaramillo, J.; Gomperts, R.; Stratmann, R. E.; Yazyev, O.; Austin, A. J.; Cammi, R.; Pomelli, C.; Ochterski, J. W.; Ayala, P. Y.; Morokuma, K.; Voth, G. A.; Salvador, P.; Dannenberg, J. J.; Zakrzewski, V. G.; Dapprich, S.; Daniels, A. D.; Strain, M. C.; Farkas, O.; Malick, D. K.; Rabuck, A. D.; Raghavachari, K.; Foresman, J. B.; Ortiz, J. V.; Cui, Q.; Baboul, A. G.; Clifford, S.; Cioslowski, J.; Stefanov, B. B.; Liu, G.; Liashenko, A.; Piskorz, P.; Komaromi, I.; Martin, R. L.; Fox, D. J.; Keith, T.; Al-Laham, M. A.; Peng, C. Y.; Nanayakkara, A.; Challacombe, M.; Gill, P. M. W.; Johnson, B.; Chen, W.; Wong, M. W.; Gonzalez, C.; Pople, J. A. *Gaussian 03*, revision B.02; Gaussian, Inc.: Pittsburgh, PA, 2003.

(10) Warneck, P. *Z. Naturforsch A.* **1971**, *26*, 2047.

(11) Guyon, P. M.; Chupka, W. A.; Berkowitz, J. *J. Chem. Phys.* **1976**, *64*, 1419.

(12) Traeger, J. C. *Int. J. Mass Spectrom. Ion Processes* **1985**, *66*, 271.

(13) Laaksonen, L. gOpenMol, 2.2 ed.; Espoo, Finland, 2002; www.c-sc.fi/gopenmol/.

(14) Press, W. H.; Teukolsky, S. A.; Vetterling, W. T.; Flannery, B. P. *Numerical Recipies in C. The Art of Scientific Computing*, 2nd ed.; Cambridge University Press: Cambridge, 1992.

(15) Levine, R. D.; Bernstein, R. B. *Molecular Reaction Dynamics and Chemical Reactivity*; Oxford University Press: New York, 1987.

(16) Lu, D.-h.; Hase, W. L. *J. Chem. Phys.* **1988**, *89*, 6723.

(17) Miller, W. H.; Hase, W. L.; Darling, C. L. *J. Chem. Phys.* **1989**, *91*, 2863.

(18) Lias, S. G.; Bartmess, J. E.; Liebman, J. F.; Holmes, J. L.; Levin, R. D.; Mallard, W. G. *J. Phys. Chem. Ref. Data* **1988**, *17*, 1.

(19) Lias, S. G. Ionization Energy Evaluation. In *NIST Standard Reference Database Number 69*; Linstrom, P. J., Mallard, W. G., Eds.; National Institute of Standards and Technology: Gaithersburg, MD, 2003; http://webbook.nist.gov.

(20) Sokolov, A. V.; Yavuz, D. D.; Walker, D. R.; Yin, G. Y.; Harris, S. E. *Phys. Rev. A* **2001**, *63*, 051801.

(21) Liu, J.; Kim, H.-T.; Anderson, S. L. *J. Chem. Phys.* **2001**, *114*, 9797.

(22) Niu, B.; Shirley, D. A.; Bai, Y. *J. Chem. Phys.* **1993**, *98*, 4377.

(23) Niu, B.; Shirley, D. A.; Bai, Y. *J. Chem. Phys.* **1993**, *98*, 4377.